Domain wall conduction in multiaxial ferroelectrics

Eugene A. Eliseev, Anna N. Morozovska, George S. Svechnikov, Peter Maksymovych, and Sergei V. Kalinin

Domain wall conduction in multiaxial ferroelectrics

Eugene A. Eliseev[1,2], Anna N. Morozovska[1][*], George S. Svechnikov[1],

Peter Maksymovych[3] and Sergei V. Kalinin[3][†]

[1] Institute of Semiconductor Physics, National Academy of Science of Ukraine,

41, pr. Nauki, 03028 Kiev, Ukraine

[2] Institute for Problems of Materials Science, National Academy of Science of Ukraine,

3, Krjijanovskogo, 03142 Kiev, Ukraine

[3] Center for Nanophase Materials Science, Oak Ridge National Laboratory,

Oak Ridge, TN, 37831

Abstract

The conductance of domain wall structures consisting of either stripes or cylindrical domains in multi-axial ferroelectric-semiconductors is analyzed. The effects of the flexoelectric coupling, domain size, wall tilt and curvature, on charge accumulation, are analyzed using the Landau-Ginsburg Devonshire (LGD) theory for polarization vector combined with Poisson equation for charge distributions. The proximity and size effect of the electron and donor accumulation/depletion by thin stripe domains and cylindrical nanodomains are revealed. In contrast to thick domain stripes and thicker cylindrical domains, in which the carrier accumulation (and so the static conductivity) sharply increases at the domain walls only, small nanodomains of radius less then 5-10 correlation length appeared conducting across entire cross-section. Implications of such conductive nanosized channels may be promising for nanoelectronics.

[*] morozo@i.com.ua

[†] sergei2@ornl.gov

1. Introduction

Ferroelectric domain walls were recently shown to act as conductive channels in ferroelectric-dielectrics and ferroelectric-semiconductors even at room-temperature, providing experimental counterparts to decade-old theoretical predictions [1]. Experimental results in materials such as $BiFeO_3$ [2, 3]. $Pb(Zr,Ti)O_3$ [4], SbSJ [5] and $LiNbO_3$ doped with MgO [6], all enabled by the development of scanning probe microscopy techniques capable of probing the conductance on the nanoscale, suggest the universality of this behavior. These results present an obvious interest for fundamental studies of ferroics and low-dimensional systems, as well as offer new possibilities for oxide nanoelectronics due to nanoscale dimensions of conducting entities and the possibility to control their spatial location by external fields [4]. However, for a given ferroelectric material, the wall conductivity should depend on the wall tilt, local strains (due to electrostriction), and proximity effects. These factors in turn determine the possibility for multilevel storage, device size, and integration into solid-state devices. Thus the understanding of the role of these effects on wall conductivity is a required first step in analyzing the feasibility of controllable rewritable conductive nanosized channels design in otherwise insulating ferroelectrics.

I. Historical overview

Below we summarize the existing literature on the domain wall conductance in uniaxial ferroelectrics, wall structure in multiaxial ferroics, and mechanisms of coupling between order parameters and strain, which are relevant to the analysis of the wall conductance.

I.1. Wall conductance in uniaxial ferroelectrics

Recent reviews of up-to-date theoretical achievements in the field of domain structures in ferroics could be found in many textbooks (see e.g. [7, 8]). Briefly, the consistent studies of ferroelectric domain wall (DW) began with seminal papers of Zhirnov [9], Cao and Cross [10], who considered 180- and 90-degree DWs, taking into account electrostriction coupling between the spontaneous polarization and strain, but considering only electro-neutral DW. The case of rhombohedral symmetry is considered in Ref. [11]. Note, that orientation of 180 degree DW is determined by electrostatics, while orientation of 90-degree twin DW is mainly governed by the strain compatibility [9, 10, 12].

Earlier results on domains in uniaxial ferroelectric-semiconductors are summarized in Ref. [13], recent studies [14] and [15] are devoted to the perpendicular (or "counter") and inclined DW respectively. The static conductivity of domain walls with different incline angle with respect to spontaneous polarization vector was calculated numerically in the uniaxial ferroelectrics-semiconductors of *n*-type [15]. Unexpectedly, the static conductivity drastically increases at the inclined head-to-head wall by an order of magnitude for small incline angles and by 3 orders of

magnitude for the perpendicular domain wall due to strong accumulation of compensating free charges.

At the same time the study of DW structure and conductance in multiaxial ferroelectrics is much more complicated, since there are several components of the order parameter, which should be mixed at the DW through strain, biquadratic coupling term and flexoelectric effect as discussed below.

I.2. Wall structure in multiaxial ferroics

For multiaxial ferroics with multicomponent order parameters, analysis of polarization structure at the domain wall necessitates taking into account the relevant coupling between order parameter components (e.g. for the boundary between 90-degree DWs or some type of 180-degree DWs in incipient ferroelectrics [16]), mediated by stress accommodation or gradients coupling. For instance, the bi-quadratic coupling term for two order parameters, also known as Houchmandzadeh-Lajzerowicz-Salje coupling [17], was introduced to describe the coupling between polarization and a structural order parameter (see Ref.[18] for typical case of PZT). This coupling can lead to the appearance of polarization on structural domains (twins), however the conditions of such manifestations are usually very strict [16]. Situation is similar for ferromagnetics-ferroelectrics, where local magnetic moment is possible at the ferroelectric DW due to either biquadratic [19] or inhomogeneous coupling [20, 21].

Despite the very early attempts to describe polarization behavior in multicomponent ferroics [9, 10, 22], the progress toward understanding of their DW structure appears to be very limited. Only recently Hlinka and Márton [23] calculated numerically the structure of twin boundaries in tetragonal perovskite crystal $BaTiO_3$ in the framework of the phenomenological LGD model. They found that the polarization component normal to DW demonstrates a weak deviation from constant distribution, in contrast to the previous studies of Zhirnov [9], Cao and Cross [10]. This leads to the appearance of internal electric field and thus to a potential step at the DW, which is consistent with *ab initio* calculations [24]. Ferroelectric DWs resembling Neel walls in ferromagnetics were predicted in thin ferroelectric films [25] and incipient ferroelectrics [16, 26].

I.3. Flexoelectric effect on domain wall structure

It should be noted that none of the previous theoretical studies predict normal component of polarization at the nominally neutral 180-degree domain walls in the bulk ferroelectrics. At the same time the flexoelectric coupling can break the wall symmetry and induce the normal component of polarization along 180-degree DW [4]. Flexoelectric effect describes the coupling of polarization with strain gradient and polarization gradient with the strain [27, 28, 29]. It was first predicted by Mashkevich and Tolpygo [30]. Subsequently, a number of theoretical studies of the flexoelectric effect in conventional [31, 32, 33, 34, 35, 36, 37, 38] and incipient [39] ferroelectrics have been performed.

3

Experimental measurements of the flexoelectric tensor components were recently carried out by Ma and Cross [40, 41, 42] and Zubko et al [43]. Recently a very high value of flexoelectric coupling coefficient was reported [44] for a polar phase of polyvinylidene fluoride films.

It is generally believed that the main consequence of the flexoelectric coupling is the renormalization of the polarization gradient energy (see e.g. [16, 31, 37]). In addition, some unusual coupling terms originated from the flexoelectric effect in nanosystems [37, 45]. Notably, the flexoelectric coupling could not be ignored in the presence of inhomogeneous strains/stress, and hence becomes relevant in the vicinity of the surfaces/interfaces and domain walls.

Here we explore the polarization structure and transport behavior at the domain walls in the *multiaxial* ferroelectrics like $BiFeO_3$ and $Pb(Zr,Ti)O_3$ determined by the interplay of the strong flexoelectric coupling between polarization components and inhomogeneous elastic strains along the walls. The paper is organized as follows. Basic equations are listed and discussed in the Section 2. The impact of flexoelectric coupling and tilt angle on the polarization vector, potential, electric field and carrier redistribution across the stripe domains is analyzed in the Section 3.1. The impact of the flexoelectric coupling, proximity and finite size effect on the polarization vector, potential, electric field and carrier redistribution across the thin stripes and cylindrical nanodomains is analyzed in the Sections 3.2 and 3.3 correspondingly. Section 4 is a brief summary.

2. Basic equations

Here we analyze the space charge accumulation by various ferroelectric domain walls using LGD formalism. The free energy density is:

$$G = \Delta G_b + \Delta G_{elast} + \Delta G_{strict} + \Delta G_{flexo} - P_i \frac{E_i^d}{2} + \frac{g_{ijkl}}{2} \frac{\partial P_i}{\partial x_j} \frac{\partial P_k}{\partial x_l} \qquad (1)$$

P_i (*i*=1-3) is the ferroelectric polarization vector components. $E_i^d = -\partial\varphi/\partial x_i$ are the components of depolarization field, that is caused by imperfect screening of the inhomogeneous polarization distribution with $\text{div}(\mathbf{P}) \neq 0$. The fourth-rank symmetric tensor of gradient energy, g_{ijkl}, is positively defined for commensurate ferroelectrics considered hereinafter. Note, that the symmetrical part of the matrix $(\partial P_i/\partial x_j)(\partial P_k/\partial x_l)$ contributes to the gradient energy of the bulk system [23].

Below we consider the systems with parent high temperature phase of m3m symmetry (e.g. for tetragonal, orthorhombic, and rhombohedral low temperature ferroic phases). The Voigt notations will be used hereinafter for all those pairs of tensorial indexes, for which the tensor is symmetric with respect to their permutation. In Voigt notations 1=11, 2=22, 3=33, 4=23, 5=13, 6=12. In particular, only the components g_{11}, g_{12} and g_{44} matter for the systems with m3m symmetry [23].

The polarization-dependent density ΔG_b can be written as a Taylor series expansion of the polarization components P_i as [10]:

$$\Delta G_b = a_1\left(P_1^2 + P_2^2 + P_3^2\right) + a_{11}\left(P_1^4 + P_2^4 + P_3^4\right) + a_{12}\left(P_1^2 P_2^2 + P_2^2 P_3^2 + P_3^2 P_1^2\right) + a_{111}\left(P_1^6 + P_2^6 + P_3^6\right)$$
$$+ a_{112}\left[P_1^4\left(P_2^2 + P_3^2\right) + P_2^4\left(P_3^2 + P_1^2\right) + P_3^4\left(P_1^2 + P_2^2\right)\right] + a_{123}\left(P_1^2 P_2^2 P_3^2\right) \tag{2}$$

Here a_i, a_{ij} and a_{ijk} are the dielectric stiffness and higher-order stiffness coefficients at constant stress written in the Voigt notations. The elastic energy in Eq.(1) is

$$\Delta G_{elast} = -\frac{1}{2}s_{11}\left(\sigma_1^2 + \sigma_2^2 + \sigma_3^2\right) - s_{12}\left(\sigma_1\sigma_2 + \sigma_2\sigma_3 + \sigma_3\sigma_1\right) - \frac{1}{2}s_{44}\left(\sigma_4^2 + \sigma_5^2 + \sigma_6^2\right) \tag{3}$$

Here σ_i are the stress tensor components; s_{ij} are the elastic compliances at constant polarization written in the Voigt notations.

The coupling energy between polarization and strain ΔG_{strict} is proportional to electrostriction coefficients:

$$\Delta G_{strict} = \begin{pmatrix} -Q_{11}\left(\sigma_1 P_1^2 + \sigma_2 P_2^2 + \sigma_3 P_3^2\right) - Q_{44}\left(\sigma_4 P_2 P_3 + \sigma_5 P_3 P_1 + \sigma_6 P_1 P_2\right) \\ -Q_{12}\left(\sigma_1\left(P_2^2 + P_3^2\right) + \sigma_2\left(P_3^2 + P_1^2\right) + \sigma_3\left(P_1^2 + P_2^2\right)\right) \end{pmatrix} \tag{4}$$

where Q_{ij} is the electrostriction strain tensor written in the Voigt notations.

The short form of the flexoelectric coupling contribution for a bulk material is [16]:

$$\Delta G_{flexo} = F_{11}\left(\sigma_1\frac{\partial P_1}{\partial x_1} + \sigma_2\frac{\partial P_2}{\partial x_2} + \sigma_3\frac{\partial P_3}{\partial x_3}\right) +$$
$$+ F_{12}\left(\sigma_2\frac{\partial P_1}{\partial x_1} + \sigma_1\frac{\partial P_2}{\partial x_2} + \sigma_1\frac{\partial P_3}{\partial x_3} + \sigma_3\frac{\partial P_1}{\partial x_1} + \sigma_2\frac{\partial P_3}{\partial x_3} + \sigma_3\frac{\partial P_2}{\partial x_2}\right) \tag{5}$$
$$+ F_{44}\left(\sigma_4\frac{\partial P_3}{\partial x_2} + \sigma_4\frac{\partial P_2}{\partial x_3} + \sigma_5\frac{\partial P_1}{\partial x_3} + \sigma_5\frac{\partial P_3}{\partial x_1} + \sigma_6\frac{\partial P_2}{\partial x_1} + \sigma_6\frac{\partial P_1}{\partial x_2}\right)$$

Flexoelectric effect tensor is denoted as F_{ik}. Full form of Eq.(5) valid for both finite systems and bulk materials is rather cumbersome (see Eq.(A.1) in the **Appendix A** of EPAPS [46]).

The electrostatic potential, φ, satisfies the Poisson equation

$$\varepsilon_0\varepsilon_b\Delta\varphi = \mathrm{div}(\mathbf{P}) - e\left(N_d^+(\varphi) + p(\varphi) - n(\varphi) - N_a^-\right) \tag{6}$$

Here Δ is the Laplace operator, the charges are in the units of electron charge $e=1.6\times10^{-19}$ C, $\varepsilon_0=8.85\times10^{-12}$ F/m is the universal dielectric constant, ε_b is the background dielectric permittivity of the material (unrelated with the soft mode), that is typically much smaller than the ferroelectric permittivity ε_{ij}^f related with the soft mode. Note that the ferroelectric permittivity is already included in Eq.(6) from the term $\mathrm{div}(\mathbf{P})$, when ferroelectric polarization can be approximated as expansion $P_i = P_i^S + \varepsilon_{ij}^f E_j + \ldots$.

Ionized deep acceptors with field-independent concentration N_a^- play the role of a background charge. The equilibrium concentrations of ionized shallow donors N_d^+ (e.g. vacancies), free electrons n and holes p are:

$$N_d^+(\varphi) = N_{d0}\left(1 - f\left(E_d - E_F - e\varphi\right)\right), \tag{7a}$$

$$p(\varphi) = \int_0^\infty d\varepsilon \cdot g_p(\varepsilon) f\left(\varepsilon - E_V + E_F + e\varphi\right), \tag{7b}$$

$$n(\varphi) = \int_0^\infty d\varepsilon \cdot g_n(\varepsilon) f\left(\varepsilon + E_C - E_F - e\varphi\right). \tag{7c}$$

Where N_{d0} is the concentration of donors, $f(x) = \left\{1 + \exp(x/k_B T)\right\}^{-1}$ is the Fermi-Dirac distribution function, $k_B = 1.3807 \times 10^{-23}$ J/K, T is the absolute temperature. E_F is the Fermi level, E_d is the donor level, E_C is the bottom of conductive band, E_V is the top of the valence band (all energies are defined with respect to the vacuum level). The electron and hole density of states in the effective mass approximation are $g_n(\varepsilon) \approx \dfrac{\sqrt{2 m_n^3 \varepsilon}}{2\pi^2 \hbar^3}$ and $g_p(\varepsilon) \approx \dfrac{\sqrt{2 m_p^3 \varepsilon}}{2\pi^2 \hbar^3}$, respectively. Typically the condition $m_n \ll m_p$ is satisfied.

Assuming that a single domain ferroelectric material is electroneutral at zero potential $\varphi = 0$, the condition $N_a^- = N_{d0}^+ + p_0 - n_0$ should be valid. The equilibrium concentration of donors is $N_{d0}^+ = N_{d0}\left(1 - f\left(E_d - E_F\right)\right) \equiv N_{d0} f\left(E_F - E_d\right)$, equilibrium densities of holes $p_0 = \int_0^\infty d\varepsilon \cdot g_p(\varepsilon) f\left(\varepsilon + E_F - F_V\right)$ and electrons $n_0 = \int_0^\infty d\varepsilon \cdot g_n(\varepsilon) f\left(\varepsilon + E_C - F_F\right)$ are defined for the case $\varphi = 0$.

Since the quasi-one dimensional distribution of polarization and stresses depend only on the distance from the wall plane in the vicinity of the domain walls, it is convenient to go to a new coordinate system, with $\tilde{x}_1$ axis normal to the domain wall plane $\{\tilde{x}_2, \tilde{x}_3\}$ instead of the coordinate system $\{x_1, x_2, x_3\}$ with axes along the cubic symmetry axes [**Figs.1a**]. Rotations of crystallographic reference frame to the coordinate system, associated with the domain wall, are defined by the angles $\{\theta, \phi\}$. Components of any vector (e.g. polarization, field) and tensor (e.g. stress) in the new coordinate system could be written as $\tilde{\mathbf{P}} = \mathbf{A}\,\mathbf{P}$, $\tilde{\mathbf{E}}^d = \mathbf{A}\,\mathbf{E}^d$ and $\tilde{\hat{\mathbf{X}}} = \mathbf{A}\,\hat{\mathbf{X}}\,\mathbf{A}^{\mathrm{T}}$ in the matrix form, where the transformation matrix

$$\mathbf{A} = \begin{pmatrix} \cos\theta\cos\phi & \cos\theta\sin\phi & \sin\theta \\ -\sin\phi & \cos\phi & 0 \\ -\sin\theta\cos\phi & -\sin\theta\sin\phi & \cos\theta \end{pmatrix} \tag{8}$$

Here the transposed matrix $\mathbf{A}^{\mathrm{T}}$ is inverse to the matrix $\mathbf{A}$. Inverse transformations are $\mathbf{P} = \mathbf{A}^{\mathrm{T}}\widetilde{\mathbf{P}}$, $\mathbf{E}^d = \mathbf{A}^{\mathrm{T}}\widetilde{\mathbf{E}}^d$ and $\hat{\mathbf{X}} = \mathbf{A}^{\mathrm{T}}\hat{\widetilde{\mathbf{X}}}\,\mathbf{A}$. Contribution of the inhomogeneous strains $\widetilde{u}_i$ to the free energy can be evaluated as:

$$\widetilde{G} = G + \widetilde{\sigma}_i \widetilde{u}_i \qquad (9)$$

Corresponding equations of state are $\dfrac{\partial \widetilde{G}}{\partial \widetilde{P}_i} = 0$ and $\dfrac{\partial \widetilde{G}}{\partial \widetilde{\sigma}_i} = 0$.

Additional constraints on the system are given by mechanical equilibrium conditions: $\partial\widetilde{\sigma}_1(\widetilde{x}_1)/\partial x_i = 0$, $\partial\widetilde{\sigma}_5(\widetilde{x}_1)/\partial x_i = 0$, and $\partial\widetilde{\sigma}_6(\widetilde{x}_1)/\partial x_i = 0$ compatibility relations [47]. Elastic stresses should vanish far from the domain walls, where the system is mechanically free. Other boundary conditions are determined by the configuration of the domain structure in a straightforward way. In particular, the potential $\varphi(\widetilde{x}_1)$ vanishes far from the domain walls and reaches maximum at the walls, so the depolarization field component $\widetilde{E}_1$ normal to the domain wall plane is zero at the wall: $\widetilde{E}_1(\widetilde{x}_1 = 0) = 0$. Polarization components $\widetilde{P}_i$ are zero at the wall plane.

In the next sections we analyze the cases of a tilted domain stripes [**Figs.1b**], parallel domain stripes [**Figs.1c**] and a single cylindrical domain [**Figs.1d**] assuming the one-dimensional distribution of polarization in the vicinity of the domain walls.
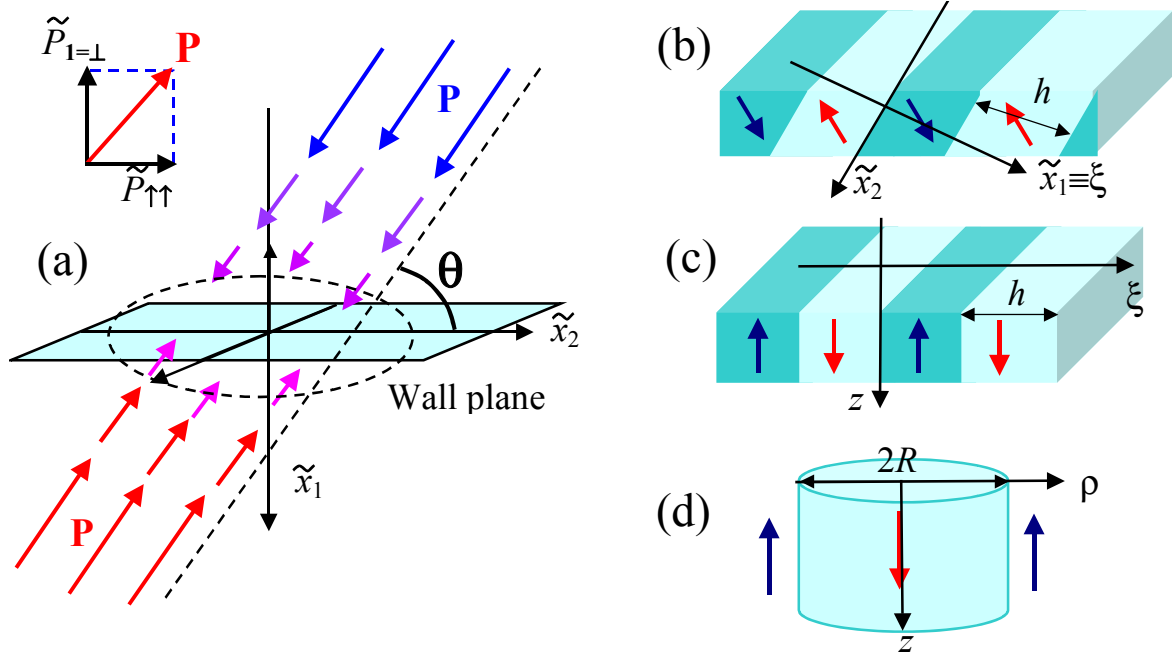

Fig. 1. (Color online) One dimensional distribution of polarization in the vicinity of a single domain wall (a), tilted (b) and parallel (c) domain stripes with half-period h; (d) cylindrical domain of radius R. Arrows in plots b-d indicate the polarization direction in the center of domains.

We note that zig-zag instabilities can appear at the charged wall plane in order to minimize its electrostatic energy [48]. However, here we consider only the cases for which the quasi-one dimensional distribution of polarization (periodic domain stripes, cylindrical domains, etc.) and leave the question of wall stability to further studies [49].

3. Results and discussion

3.1. Carriers accumulation on 180-degree domain stripes

Here we consider the effect of the flexoelectric coupling on the carriers redistribution in a tilted stripe domain structure, consisting of thin 180-degree domains with half-period h that is much higher than a correlation length, $r_c = \sqrt{-g_{44}/2a_1}$. The planes $\xi = nh$ ($n = 0, \pm 1, \pm 2, ...$) correspond to the domain walls between two neighboring stripes (see **Fig.1b**). In the section we regard that $h = 100 r_c$. The condition $h \gg r_c$ allows us to focus on the impact of the wall tilt and flexoelectric coupling, while proximity effects, which are dominant for thin stripes, will be considered in the next section.

Equations of state $\dfrac{\partial \widetilde{G}}{\partial \widetilde{P}_i} = 0$, $\dfrac{\partial \widetilde{G}}{\partial \widetilde{\sigma}_i} = 0$ and the Poisson equation (6) were rewritten in dimensionless variables (see **Appendix A.2** in EPAPS [46]) and then analyzed numerically for PbZr$_{0.2}$Ti$_{0.8}$O$_3$ **(PZT)** material parameters. Material parameters for PZT used in the calculations are listed in the **Table 1**.

Table 1[*)]**.** Free energy coefficients for bulk ferroelectric PbZr$_{0.2}$Ti$_{0.8}$O$_3$ (from Refs.[50, 51]).

a_1 ($\times 10^7$C^{-2} • m^{2}N)	a_{ij} ($\times 10^8$C^{-4} • m^{6}N)	a_{ijk} ($\times 10^8$C^{-6} • m^{10}N)	Q_{ij} (C^{-2} • m^4)	s_{11} ($\times 10^{-12}$ Pa^{-1})	g_{11} ($\times 10^{-10}$C^{-2}m^{4}N)
−14.84 at 25°C	a_{11}= −0.305 a_{12}= 6.32	a_{111}=2.475 a_{112}=9.68 a_{123}= −49.01	Q_{11}=0.0814 Q_{12}= −0.0245 Q_{44}=0.0642	s_{11}=8.2 s_{12}= −2.6 s_{44}=14.4	g_{11}=2.0 g_{44}=1.0

[*)] correlation length $r_c = \sqrt{-g_{44}/2a_1}$ ≈0.5 nm, $m_n = 0.05 m_e$, $m_p = 5 m_e$, where m_e is the mass of the free electron, $\varepsilon_b = 5$, band gap $E_g = 3$ eV, $N_{d0} = 10^{25}$ m^{-3}, $E_d = 0.1$eV.

Estimations based on Ma and Cross [52] results give the flexoelectric effect coefficient $|F_{ij}| \approx (0.5-1) \times 10^{-10}$m^3/C and F_{12} is likely negative. Below we consider the flexoelectric tensor F_{ij} in the isotropic approximation ($F_{44} = F_{11} - F_{12}$). Using the elastic solution $\widetilde{\sigma}_1 = \widetilde{\sigma}_5 = \widetilde{\sigma}_6 = 0$ and isotropic approximation for F_{ij} one leads to the simple form of the flexoelectric energy (5):

$\Delta G_{flexo} = F_{12}\left(\widetilde{\sigma}_2 \dfrac{\partial \widetilde{P}_1}{\partial \widetilde{x}_1} + \widetilde{\sigma}_3 \dfrac{\partial \widetilde{P}_1}{\partial \widetilde{x}_1}\right)$, which depends on the F_{12} component only. Correlation length

$r_c \approx 0.5$ nm, coordinate $\xi \equiv \widetilde{x}_1$, spontaneous polarization P_S and thermodynamic coercive field E_{coer} are introduced.

Dependences of the polarization component perpendicular $\widetilde{P}_1(\xi) \equiv P_\perp(\xi)$ and parallel $\widetilde{P}_{\uparrow\uparrow}(\xi)$ to the wall plane, electric potential $\varphi(\xi)$, ionized donors $N_d^+(\xi)$ and electrons $n(\xi)$ on the distance ξ from the domain wall plane between the neighboring stripes are shown in **Figs. 2-3**. The dependencies were calculated for the domain stripes with different tilt angles $\theta = \pi/2,\, \pi/30,\, 0$ (red, blue and black curves respectively), negative, zero and positive flexoelectric coupling coefficient F_{12} (solid, dashed and dotted curves respectively).

Without flexoelectric coupling only electrostriction couples polarization and elastic strains. To the best of our knowledge, the effect of the flexoelectric coupling on the ferroelectric wall charge state was not studied theoretically before. Here we show that the flexoelectric coupling leads to the nontrivial physical responses, including appearance of $P_\perp(\xi)$ and its strong gradient across the "nominally uncharged" and weakly charged head-to-head (**h-t-h**) and tail-to-tail (**t-t-t**) domain walls (see curves calculated for $\theta = 0$ and $\theta = \pi/30$). Actually, the flexoelectric coupling term $F_{12}\widetilde{P}_\perp \partial(\widetilde{\sigma}_2 + \widetilde{\sigma}_3)/\partial\widetilde{x}_1$ in the free energy causes the "flexoelectric" field $F_{12} \partial(\widetilde{\sigma}_2 + \widetilde{\sigma}_3)/\partial\widetilde{x}_1$, that in turn induces the component $P_\perp(\xi)$. It is seen from the **Figs.2b-c** that $P_\perp(\xi) = 0$ for $F_{12} = 0$ and $\theta = 0$. Polarization component $P_{\uparrow\uparrow}(\xi)$ is rather weakly affected by the presence of the flexoelectric coupling (curves calculated for $F_{12} = 0$ and $F_{12} \neq 0$ almost coincide in **Figs.2d).**
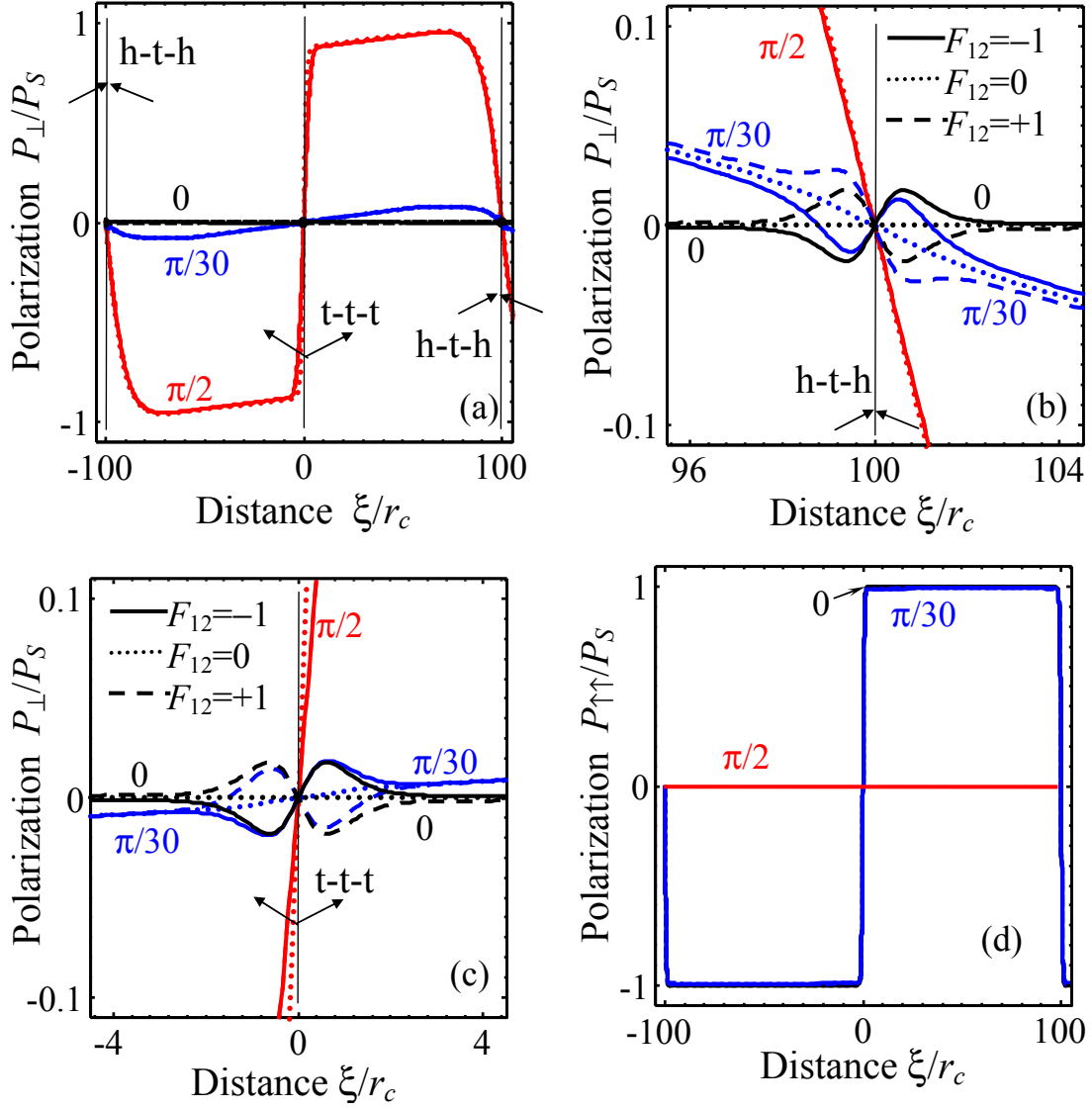
Fig. 2. (Color online) Dependencies of the polarization components $\tilde{P}_{\perp}(\xi)/P_s$ (a, c, d) and $\tilde{P}_{\uparrow\uparrow}(\xi)/P_s$ (b) on the distance ξ from the wall plane between the neighboring stripes with different tilt angle $\theta = \pi/2,\ \pi/30, 0$ (see figures near the curves). Flexoelectric coupling coefficient $F_{12} = (-0.5,\ 0,\ 0.5) \times 10^{-10} \mathrm{m}^3/\mathrm{C}$ (solid, dotted and dashed curves respectively). Material parameters correspond to PbTi$_{0.8}$Zr$_{0.2}$O$_3$ (listed in the **Table 1**), stripe half-period $h = 100 r_c$.

At zero or small tilt angle an additional features on the potential, electrons and ionized donor distributions appear in vicinity of domain walls due to the nonzero flexoelectric coupling (see **Fig.3b,d,f**). In particular the flexoelectric coupling leads to the appearance of additional electrostatic potential well/barrier depending on the sign of the flexoelectric coefficient F_{12} (see **Fig.3b**). The depth of the potential barrier well/height appeared at the wall due to $P_{\perp}(\xi)$-effect, as derived in **Appendix D** of EPAPS [46], is proportional to the flexoelectric coupling coefficient F_{12}. Note that the flexoelectric

10

coupling and tilt influence on the wall charge state is not additive. In particular the spatial localization of the features induced by the flexoelectric coupling is independent on wall tilt angle, but the width increases with decreasing angle.

The flexoelectric field leads to the carriers redistribution and thus to conductivity changes even across the nominally uncharged parallel domain walls [4]. It is seen from **Figs.3e-f** that head-to-head and tail-to-tail domain walls have different electronic properties: head-to-head walls appeared electron accumulating, while tail-to-tail walls appeared donor (e.g. vacancies) accumulating, similarly to the one-component polarization in uniaxial ferroelectrics considered in [15]. The potential barrier created by the bound charges and screening carriers are the highest for the perpendicular wall ($\theta = \pi/2$) with the maximal bound charge $2P_S$. Since the angular dependence of the bound charge is $2P_S \sin\theta$, the barrier decreases with decreasing θ. The compensating electron density is highest for the head-to-head perpendicular wall ($\theta = \pi/2$) and decreases with decreasing bound charge (i.e. with decreasing θ). The electron accumulation leads to the strong increase of the static conductivity across the charged domain stripes up 3 orders of magnitude for the perpendicular domain walls in PZT. Hole density appears less than 10^{-40}m^{-3}, i.e. free holes are almost absent near the head-to-head domain walls between the neighboring stripes.

Note, that the static electronic and ionic conductivity can be estimated as $\lambda_e(\xi) = e(\eta_e n(\xi) + \eta_p p(\xi))$ and $\lambda_i(\xi) = e\eta_d N_d^+(\xi)$, where $\eta_{e,p,d}$ are corresponding mobilities, which are regarded as constant. Since the strength of carrier accumulation/depletion at the wall plane is determined by the behavior of electric potential $\varphi(0)$ at the wall, the conductivity should be controlled by the field effect. The profile of the latter across the wall in turn depends on the wall tilt, stripe domain size, etc. **Figure 4a** shows the dependence of potential $\varphi(0)$ on the tilt angle θ calculated for head-to-head and tail-to-tail walls. The potential $\varphi(0)$ increases with increasing θ. Dependences of the electronic and ionic conductivity on the wall tilt angle θ are shown in **Fig. 4b,c** for negative, zero, and positive flexoelectric coupling coefficient. It is seen from the figure that the electronic conductivity increases and ionic conductivity decreases with θ increase for head-to-head domain walls. The electronic conductivity decreases and ionic conductivity increases and saturates with θ increase for tail-to-tail domain walls.
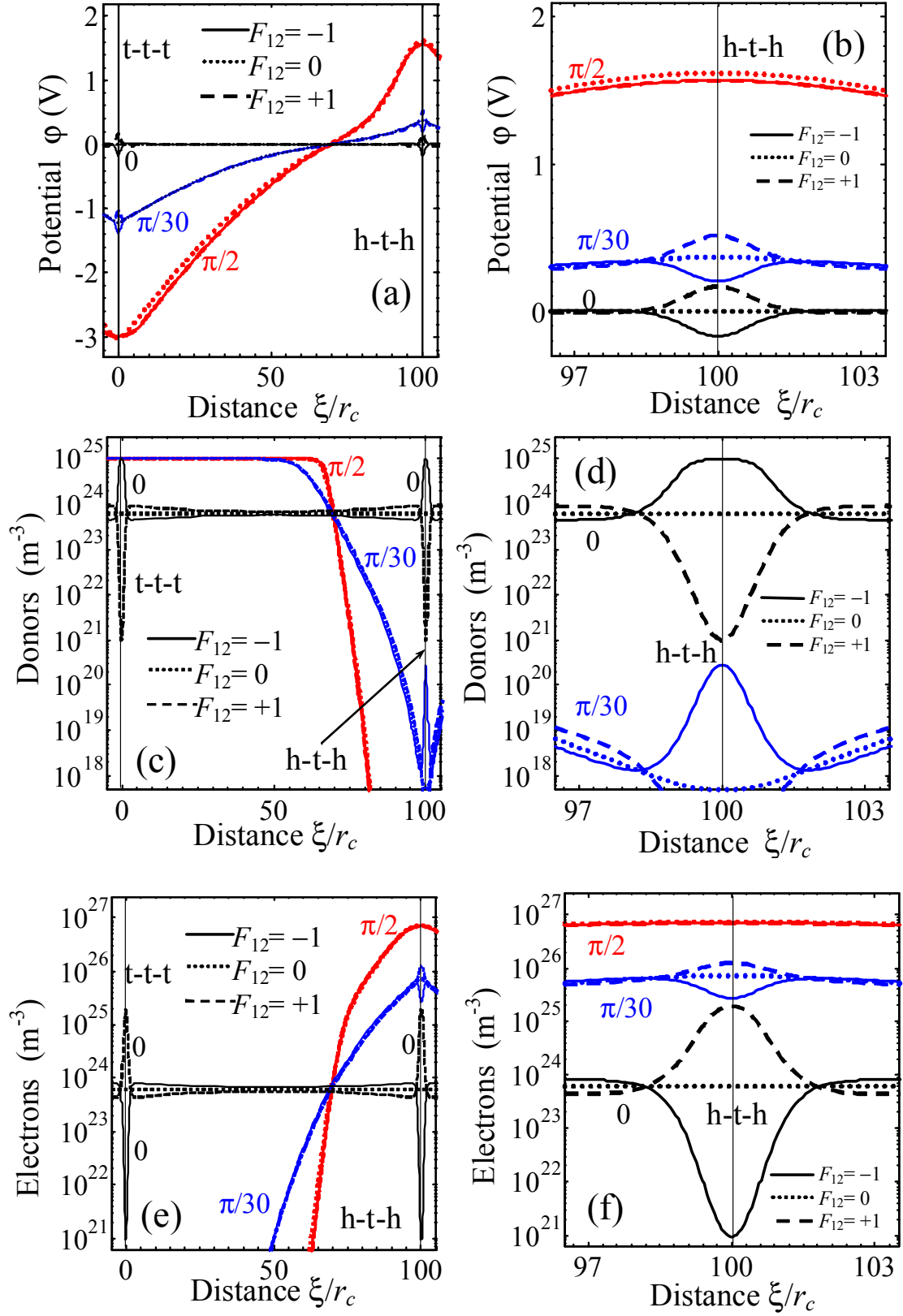
Fig. 3. (Color online) Dependencies of potential $\varphi(\xi)$ (a,b), concentration of ionized donors $N_d^+(\xi)$ (c,d) and density of electrons $n(\xi)$ (e, f) on the distance ξ from the wall plane between the neighboring stripes with different tilt angle $\theta = \pi/2, \pi/30, 0$ (see figures near the curves).

Flexoelectric coupling coefficient $F_{12} = (-0.5, 0, 0.5) \times 10^{-10} \text{m}^3/\text{C}$ (solid, dotted and dashed curves respectively). Panels (b, d, f) represent the region near the head-to head wall. Parameters are the same as in **Figs.2.**
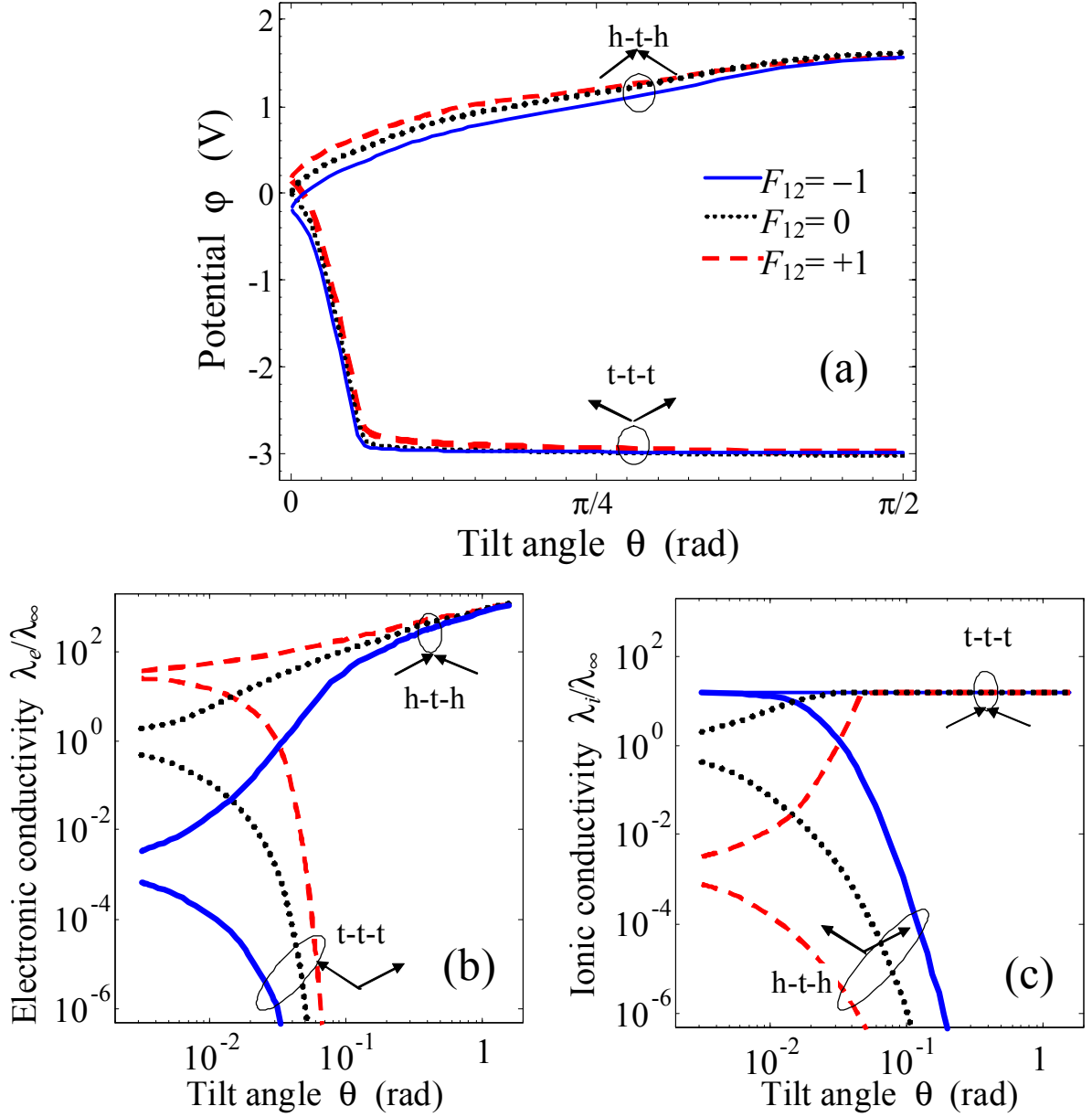

Fig. 4. (Color online) Dependence of potential $\varphi(\xi = 0)$ (a), electronic (b) and ionic (c) conductivity on the domain wall tilt angle θ between the neighboring head-to-head (h-t-h) and tail-to-tail (t-t-t) stripes and calculated for negative, zero, and positive flexoelectric coupling coefficient $F_{12} = (-0.5, 0, 0.5) \times 10^{-10} \text{m}^3/\text{C}$ (solid, dotted and dashed curves respectively). Material parameters are the same as in **Figs.2.**

To summarize the section, the free carriers accumulation leads to the strong increase of compensating charge density and thus the static conductivity across the tilted walls between stripe domains in multi-axial ferroelectrics-semiconductors of n-type: from 1 order for the parallel domain stripes due to the flexoelectric coupling up 3 orders of magnitude for perpendicular domain walls (even without flexoelectric coupling impact). **Table 2** lists some peculiarities of the domain walls conductivity in the n-type ferroelectric-semiconductors with special attention to the flexoelectric coupling. Note, that the static electronic conductivity increase should exist in the p-type ferroelectric-semiconductors across the tail-to-tail walls.

Table 2. Wall conductivity peculiarities in the n-type ferroelectric-semiconductors

flexoelectric coupling coefficient F_{12}	Conductivity of parallel and slightly tilted 180-degree domain walls (tilt angle $0 \leq \theta \ll 6^o$)	Conductivity of tilted head-to-head 180-degree walls (tilt angle $\theta > 6^o$)	Conductivity of tilted tail-to-tail 180-degree walls (tilt angle $\theta > 6^o$)
positive	up to 50-100 times higher than the bulk one due to the electron accumulation	gradually increases up to 10^2-10^3 times with the tilt angle increase due to the strong accumulation of electrons	~10 times higher than the bulk one due to the donor accumulation and saturation
zero	the same as in the bulk	gradually increases up to 10^2-10^3 times with the tilt angle increase due to the strong accumulation of electrons	~10 times higher than the bulk one due to the donor accumulation and saturation
negative	increases up to 10 times due to the donors accumulation and saturation	gradually increases up to 10^2-10^3 times with the tilt angle increase due to the strong accumulation of electrons	~10 times higher than the bulk one due the donor accumulation and saturation

3.2. Proximity effects on carrier accumulation by 180-degree stripe domains

In this section we consider thin 180-degree periodic domains of half-period h. The domain walls are parallel ($\theta=0$) and located enough close to induce proximity effects on the system static conductivity. The domain walls are considered as "nominally neutral", i.e. their polarization vector is parallel to the wall plane in the center of the domain stripe. The planes $\xi = nh$ ($n = 0, \pm 1, \pm 2, ...$) correspond to the domain wall between two neighboring stripes (see **Fig.1c**). Our calculations show that the polarization component $\widetilde{P}_\perp(\xi)$ is induced by the flexoelectric coupling. The bound charge $\widetilde{P}_\perp(\xi)$ leads to the appearance of lateral depolarization electric field $\widetilde{E}_\perp(\xi)$ and carrier redistribution in the vicinity of domain walls.

Distributions of polarization components $\widetilde{P}_{\uparrow\uparrow}(\xi)$ and $\widetilde{P}_\perp(\xi)$, depolarization electric field $\widetilde{E}_\perp(\xi)$, electrostatic potential $\varphi(\xi)$ and screening charges (electrons and donors) are shown in **Figs. 5-6** for two periods of domain stripes, assuming negative, zero and positive flexoelectric coefficient F_{12} (solid, dashed and dotted curves correspondingly). Note, that the stripe domains with a half-period

14

below minimal value $h_{cr} \sim 2r_c$ are thermodynamically unstable due to **proximity effects,** which make the domain wall energy too high. So the curves in **Fig. 5-6** are plotted for $h \geq h_{cr}$.

$\widetilde{P}_\perp(\xi)$ and $\widetilde{E}_\perp(\xi)$ are maximal in the vicinity of domain walls (i.e. at $\xi = nh \pm \sqrt{2}r_c$), equal to zero at the walls and in the center of domain stripe (i.e. at $\xi = nh$ and $\xi = nh \pm h/2$). The maximal value of polarization component is

$$\widetilde{P}_\perp^{max} \approx \pm F_{12} \varepsilon_0 \varepsilon_b \frac{(Q_{11} + Q_{12})P_S^2}{(s_{11} + s_{12})\sqrt{2}r_c}\left(1 - \frac{h_{cr}}{h}\right) \tag{10}$$

The maximal value of electric field is

$$\widetilde{E}_\perp^{max} \approx \mp F_{12} \varepsilon_0 \varepsilon_b \frac{(Q_{11} + Q_{12})P_S^2}{(s_{11} + s_{12})\sqrt{2}r_c}\left(1 - \frac{h_{cr}}{h}\right) \tag{11}$$

The maximal values $\widetilde{E}_\perp^{max}$ are reached in the points $\xi = nh \pm \sqrt{2}r_c$ ($n = 0, \pm 1, \pm 2, ...$) corresponding to the distance $\sqrt{2}r_c$ from the domain wall plane.

Here, h_{cr} is the minimal half-period of the stable domain stripe (corresponding to the critical size originating from the proximity effect). The minimal half-period is related to correlation length r_c as $h_{cr} \approx \pi r_c/2$ for $F_{12} = 0$ and $\theta = 0$.

Electric potential reaches the maximal value

$$\varphi_{max} \approx F_{12} \frac{(Q_{11} + Q_{12})P_S^2}{(s_{11} + s_{12})}\left(1 - \frac{h_{cr}}{h}\right) \tag{12}$$

at the wall planes $\xi = nh$. Note, that the expressions for $\widetilde{P}_\perp^{max}$, $\widetilde{E}_\perp^{max}$ and φ_{max} differ from the expressions listed in Ref.[4] by the factor $\left(1 - \frac{h_{cr}}{h}\right)$ originated from the proximity effect. As anticipated, $\widetilde{P}_{\uparrow\uparrow}(\xi)$ is maximal in the center of the domain stripes $\xi = nh \pm h/2$ and zero at the wall planes $\xi = nh$. Electrons and donors distributions have sharp extremum (minimum or maximum depending on the sign of F_{12}) at the wall planes $\xi = nh$.

It is seen from the **Fig. 5** and **6** that the decrease of the half-period h leads to the gradual suppression of the maximum values of the polarization components as well as to the decrease of the modulation depth of the potential and screening charges profiles. Polarization, potential, field and carrier density profiles have quasi-sinusoidal shape for thin stripes (**Fig. 6**). Anharmonicity appears and strongly increases with h increase (**Fig.5**).

The sign of compensating carriers is determined by the sigh of the flexoelectric coefficient: negative F_{12} leads to the accumulation of negative charges (electrons or acceptors), positive F_{12} leads to the accumulation of positive charges (holes, donors or vacancies) at the walls (see **Fig.5e,f** and **6e,f**).

15

The higher the F_{12} value the stronger is the carrier accumulation effect. Note, that the experimental results [40, 41, 42] show that the coefficient F_{12} is likely negative for PZT.

The possibility of the electron and donor accumulation/depletion in the vicinity of the domain stripes is demonstrated in **Figs. 7.** Carrier accumulation in the domain wall region is caused by the potential barrier $\varphi(\xi)$, that is in turn caused by the uncompensated bound charge $P_\perp(\xi)$. Dependence of the potential barrier on the stripes half-period h is shown in **Fig. 7a** for positive, zero and negative flexoelectric coupling coefficients. Potential barrier at the domain wall, $\varphi(0)$, monotonically increases with the increasing of the stripe size h and then saturates. Potential in the middle of the stripe, $\varphi(\pm h/2)$, firstly increases with h increase, reaches maximum at $h \sim 5 r_c$ and then decreases with further h increase. For thick stripes with half-period $h \gg 100 r_c$ the potential vanishes in the central region of each stripe.

To estimate the observable conductivity, local densities of electrons $n(\xi)$ and donors $N_d^+(\xi)$ were averaged across over the domain wall apparent thickness, e.g. for distance $\xi \in \{-r_c, r_c\}$ (solid curves) as well as entire the domain stripe $\xi \in \{-h, h\}$ (dashed curves). Note, that $\langle n(\xi) \rangle / n(\infty) \approx \langle \lambda_e(\xi) \rangle / \lambda_e(\infty)$ and $\langle N_d^+(\xi) \rangle / N_d^+(\infty) \approx \langle \lambda_i(\xi) \rangle / \lambda_i(\infty)$ in the framework of the model adopted here. For positive flexoelectric coupling the electronic conductivity of domain walls monotonically increases (up to 30 times in saturation in comparison with a bulk electronic conductivity $\lambda_e(\infty)$) and then saturates with the domain stripe period increase (see **Fig. 7b,c**). For negative flexoelectric coupling the ionic conductivity of domain walls monotonically increases and then saturates (up to 15 times in saturation in comparison with a bulk ionic conductivity $\lambda_i(\infty)$) with the stripe period increase. Without flexoelectric coupling the conductivity is the same as for the homogeneous monodoman region $\lambda_{e,i}(\infty)$ (see horizontal lines marked with "0").
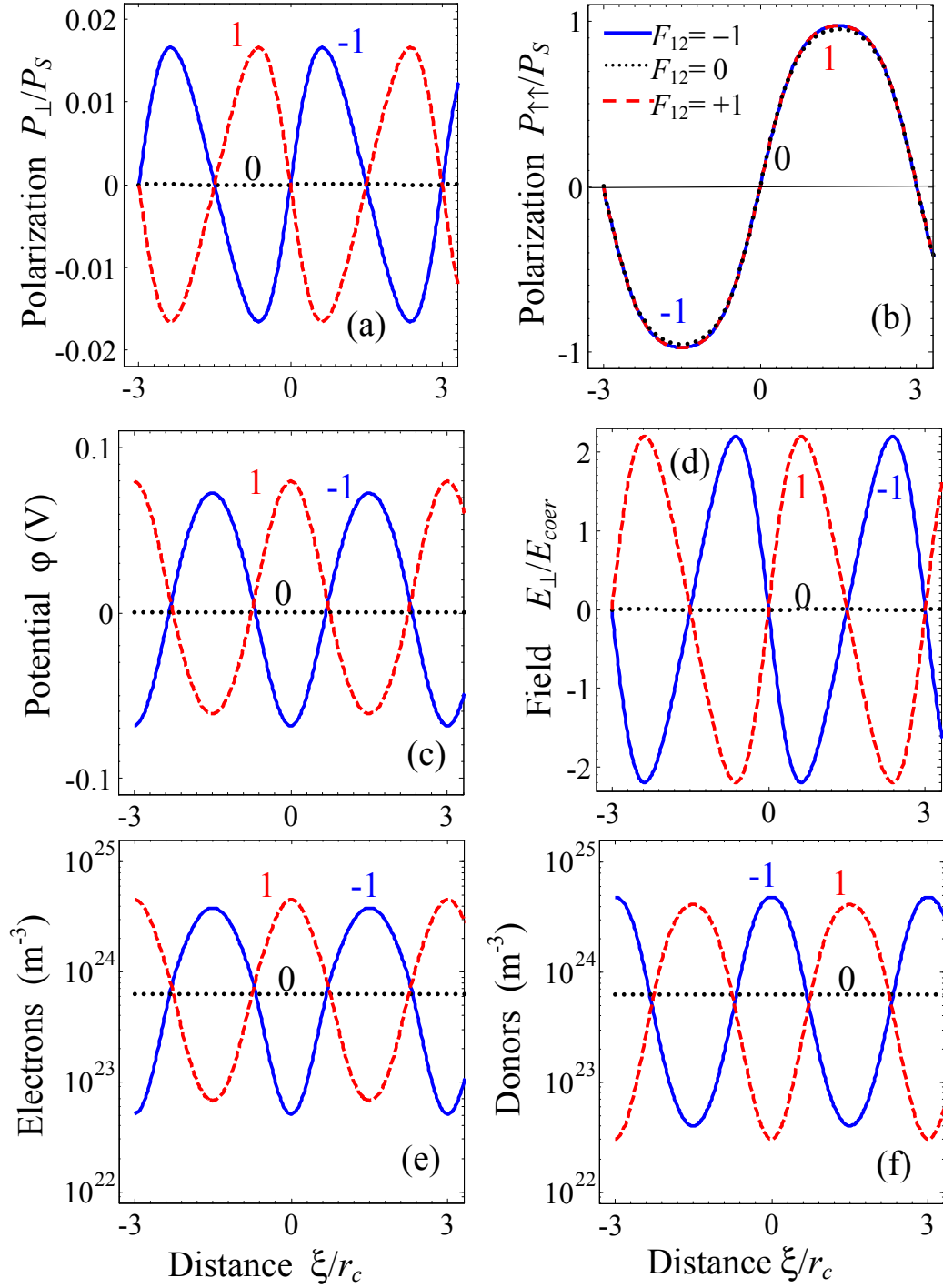
Fig. 5. (Color online) Dependencies of the polarization components $\widetilde{P}_{\perp}(\xi)/P_S$ (a) and $\widetilde{P}_{\uparrow\uparrow}(\xi)/P_S$ (b), potential $\varphi(\xi)$ (c), field $\widetilde{E}_{\perp}(\xi)/E_{coer}$ (d), electrons $n(\xi)$ (e) and ionized donors $N_d^+(\xi)$ (f) distributions on the distance ξ across the "nominally uncharged" 180-degree domain stripes (only one period is shown) calculated for the half period $h = 3r_c$ and flexoelectric coupling coefficients $F_{12} = -1 \times 10^{-10} \text{m}^3/\text{C}$ (solid curves), $F_{12} = 0$ (dotted curves) and $F_{12} = +1 \times 10^{-10} \text{m}^3/\text{C}$ (dashed curves). Other parameters are same as for **Fig. 2**.
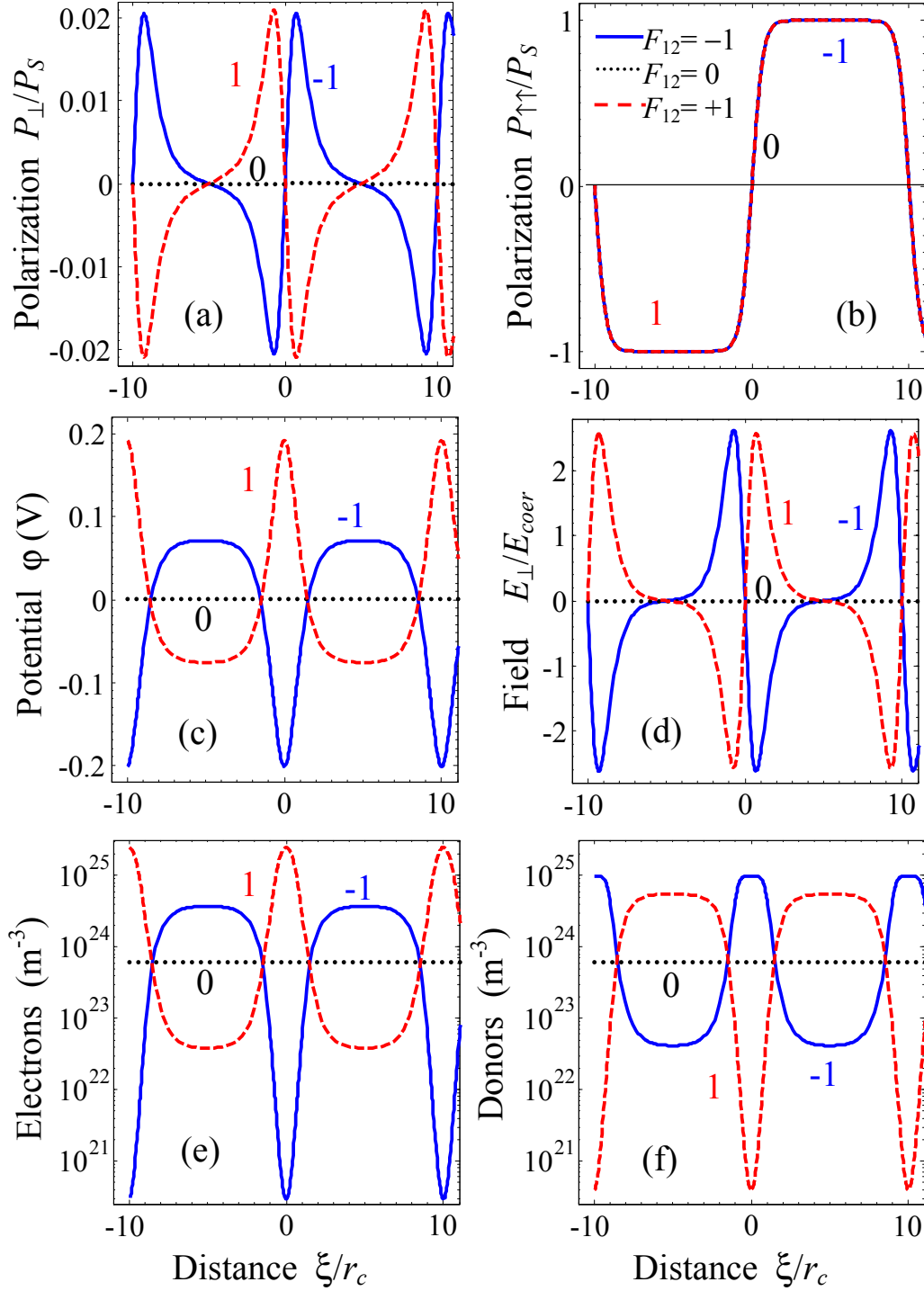
17

Fig. 6. (Color online) Dependencies of polarization components $\widetilde{P}_{\perp}(\xi)/P_S$ (a) and $\widetilde{P}_{\uparrow\uparrow}(\xi)/P_S$ (b), potential $\varphi(\xi)$ (c), field $\widetilde{E}_{\perp}(\xi)/E_{coer}$ (d), electrons $n(\xi)$ (e) and ionized donors $N_d^+(\xi)$ (f) distributions on the distance ξ across the "nominally uncharged" 180-degree domain stripes (only one period is shown) calculated for the half period $h = 10 r_c$ and flexoelectric coupling coefficients $F_{12} = -1 \times 10^{-10} m^3/C$ (solid curves), $F_{12} = 0$ (dotted curves) and $F_{12} = +1 \times 10^{-10} m^3/C$ (dashed curves). Other parameters are same as for **Fig. 2**.
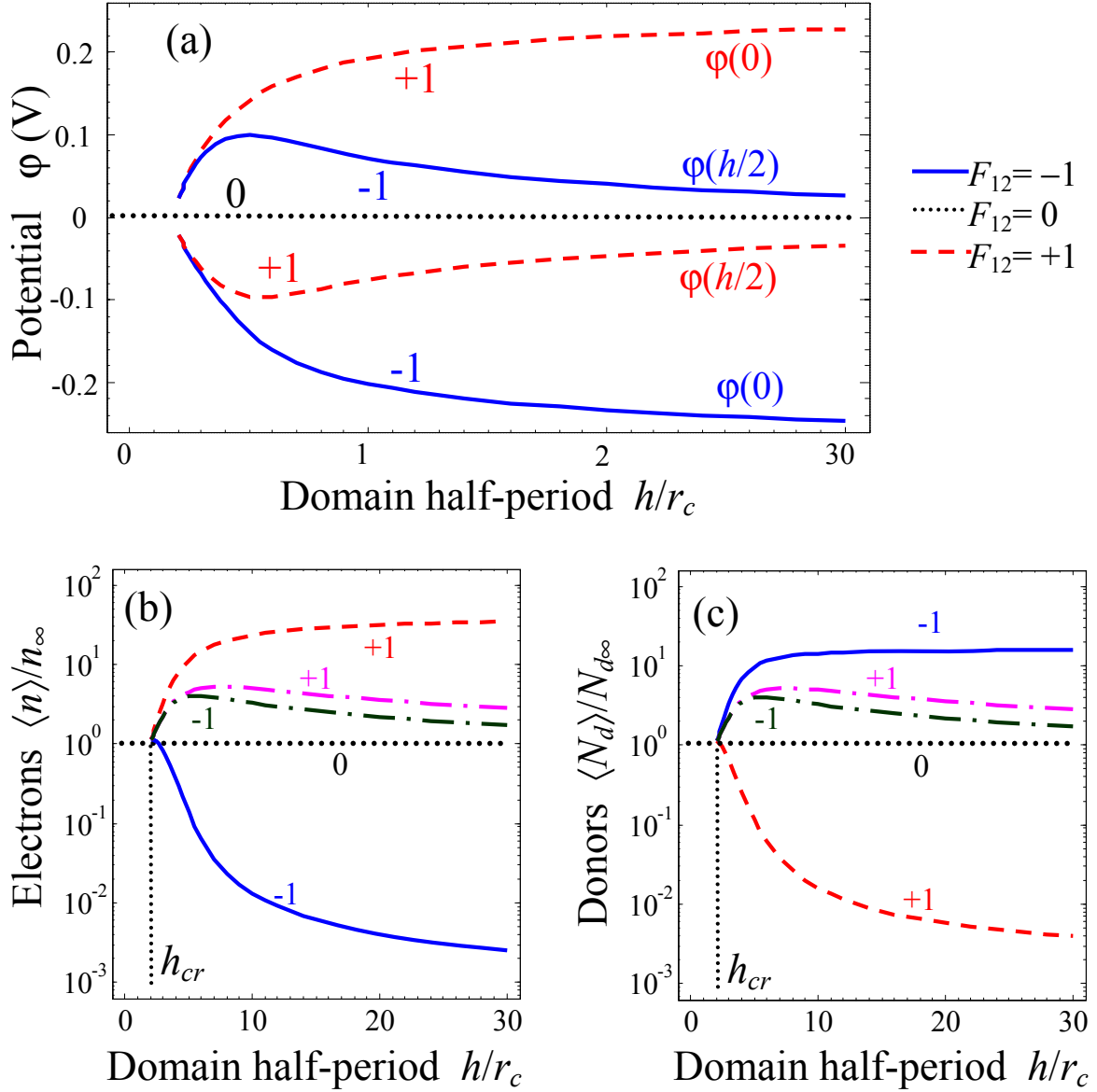
Fig. 7. (Color online) Dependence of the electric potential $\varphi(0)$ and $\varphi(h/2)$ (a), relative electron density $\langle n(\xi)\rangle/n(\infty)$ (b) and donor concentration $\langle N_d^+(\xi)\rangle/N_d^+(\infty)$ (c) on the domain stripes half-period h calculated for flexoelectric coupling coefficients $F_{12}=-1\times10^{-10}\text{m}^3/\text{C}$ (solid curves with labels "-1"), $F_{12}=0$ (dotted curves with labels "0") and $F_{12}=+1\times10^{-10}\text{m}^3/\text{C}$ (dashed curves with labels "+1"). Potential (a) is plotted at the domain wall ($\varphi(0)$) and in the middle of the stripe ($\varphi(h/2)$). Electron density $n(\xi)$ and donor concentration $N_d^+(\xi)$ were averaged across the range $\xi\in\{-r_c, r_c,\}$ (solid and dashed curves with labels "±1") as well as entire the domain cross-section $\xi\in\{-h, h\}$ (dash-dotted curves with labels "±1"). Material parameters are the same as in **Figs.2.**

Averaging over the entire domain stripe smears the impact of flexoelectric coupling sign: the dash-dotted curves are relatively close for positive $F_{12}=+1\times10^{-10}\text{m}^3/\text{C}$ and negative $F_{12}=-1\times10^{-10}\text{m}^3/\text{C}$, in contrast to very different solid and dashed curves. Independent of the F_{12} sign, the conductivity averaged entire the domain stripe firstly increase with the increasing of the stripes half-period h for very small half-periods $h_{cr}<h<5r_c$, then reaches a diffuse maximum ($\sim$ 5 times in comparison with homogeneous $\lambda_{e,i}(\infty)$) and then decreases with further h increase. The principal difference in the behavior of solid, dashed and dash-dotted curves can be explained by the following considerations. For negative F_{12} free electrons are accumulated in the immediate vicinity of the domain walls, the central regions of the stripes are depleted with electrons. For positive F_{12} the immediate vicinity of the domain walls are depleted with electrons, the central regions of the stripes accumulate electrons (see **Fig.5e and 6e**). The situation with ionized donors is visa versa: their accumulation takes place in the vicinity of domain walls for positive F_{12}, while the central regions of the stripes are depleted with donors (see **Fig.5f** and **6f**). The averaging entire the domain stripe $\xi\in\{-h,\,h\}$ contains information only about resulting depletion + accumulation effect. As anticipated, the total charge of "electrons + ionized donors" is exactly zero (i.e. the sum of the solid and dashed curves "+1" or "-1") due to the total electroneutrality in the domain structure. Due to the flexoelectric coupling, the average static conductivity of domain stripes with period $h\sim5r_c$ is significantly higher then the conductivity of monodomain region.

3.3. Carrier accumulation at the cylindrical domain wall

Cylindrical domain walls always appear at the initial stages of local polarization reversal caused by a charged SPM probe [53, 54] in ferroelectric films. In the section we consider the finite size effect of carrier accumulation and static conductivity of radially-symmetric **cylindrical domain wall** with a curvature radius R (see **Fig.1d**). Polar radius $\rho=\sqrt{x^2+y^2}$ is introduced. We assume that the cylinder axis z is pointed along one of the possible directions of spontaneous polarization. Note that for other orientations of polarization the problem could not be considered as quasi-one dimensional. Furthermore, only the case of small radii $R\le10r_c$ is of interest, since for larger radii the behavior is very similar to those obtained in the section 3.1 for the thick domain stripes.

Our numerical analysis shows that the polarization component $\widetilde{P}_{\perp}(\rho)$ and depolarization electric field $\widetilde{E}_{\perp}(\rho)$ are induced due to the flexoelectric coupling. The bound charge $\widetilde{P}_{\perp}(\rho)$ leads to the $\widetilde{E}_{\perp}(\rho)$ appearance, which causes carriers redistribution across the cylindrical domain wall. The distributions of polarization components $\widetilde{P}_{z}(\rho)$ and $\widetilde{P}_{\perp}(\rho)$, electric field $\widetilde{E}_{\perp}(\rho)$, electrostatic potential

$\varphi(\rho)$ and screening charges are shown in **Fig. 8** for two domain radii ($R=1.5r_c$ and $R=5r_c$), positive, zero and negative flexoelectric coupling coefficient F_{12}. Note, that the cylindrical domain with radius below critical value $R_{cr} \sim 1.2r_c$ is thermodynamically unstable due to **finite size effect**, so the curves in **Fig. 8** are plotted for the values $R \geq R_{cr}$.

$\widetilde{P}_\perp(\rho)$ and $\widetilde{E}_\perp(\rho)$ are maximal in the vicinity of domain walls (i.e. at $\rho = R - \sqrt{2}r_c$), zero at the walls and in the center of cylindrical domain. The maximal value of the component $\widetilde{P}_\perp(\rho)$ is

$$\widetilde{P}_\perp^{\max} \approx \pm F_{12}\varepsilon_0\varepsilon_b \frac{(Q_{11}+Q_{12})P_S^2}{(s_{11}+s_{12})\sqrt{2}r_c}\left(1-\frac{R_{cr}}{R}\right) \tag{13}$$

The maximal value of electric field is

$$\widetilde{E}_\perp^{\max} \approx \mp F_{12}\varepsilon_0\varepsilon_b \frac{(Q_{11}+Q_{12})P_S^2}{(s_{11}+s_{12})\sqrt{2}r_c}\left(1-\frac{R_{cr}}{R}\right) \tag{14}$$

Electric potential reaches the maximal value

$$\varphi_{\max} \approx F_{12}\frac{(Q_{11}+Q_{12})P_S^2}{(s_{11}+s_{12})}\left(1-\frac{R_{cr}}{R}\right) \tag{15}$$

in the center of domain for small domains (e.g. nanodomains). Note, that the expressions for $\widetilde{P}_\perp^{\max}$, $\widetilde{E}_\perp^{\max}$ and $\varphi_{\max}$ differ from the expressions listed in Ref.[4] by the factor $\left(1-\frac{R_{cr}}{R}\right)$ originated from the finite size effect. As anticipated, $\widetilde{P}_z$ is maximal in the center of cylindrical domain and zero at its boundary $\rho = R$.

It is seen from the **Figs.8a-b** that the decrease of the domain radius R leads to the suppression of the polarization component maxima as well as to the decrease of the modulation depth of the potential and screening charges profiles along the domain cross-section. Polarization, potential, field and carries density profiles have sinusoidal shape for small domains with $R = 1.5r_c$ (see **Figs.8a-f**). Deviation from the sinusoidal shape appears at $R > 2r_c$ and strongly increases with increasing R. It is seen from **Figs.8e,f** that either electron or donor accumulation takes place in the nanodomain depending on the F_{12} sign and spontaneous polarization direction. In contrast to thick domain stripes and thicker cylindrical domains, in which the carrier accumulation (and so the static conductivity) sharply increases at the domain walls only, thin nanodomains of radius $R \leq 5r_c$ can be conducting entire their cross-section.
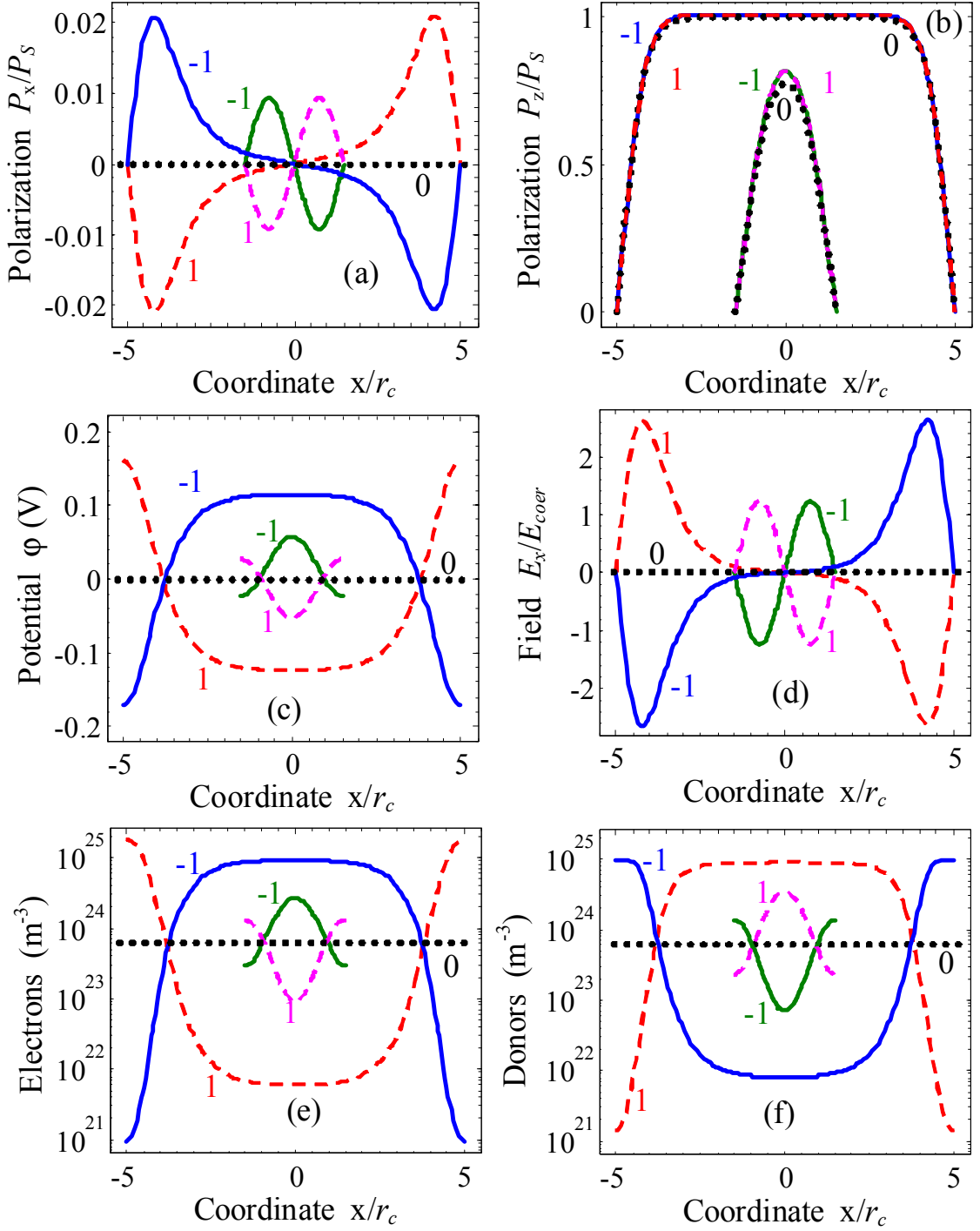
Fig. 8. (Color online) Distributions of the polarization components $P_x(x)/P_S$ (a) and $P_z(x)/P_S$ (b), potential $\varphi(x)$ (c), field $E_x(x)/E_{coer}$ (d), electron density $n(x)$ (e) and ionized donor concentration $N_d^+(x)$ (f) along the cross-section of cylindrical domains with radii $R = 1.5r_c$ (magenta and green curves) and $R = 5r_c$ (red and blue curves) calculated for flexoelectric coupling coefficients $F_{12} = -1 \times 10^{-10} \text{m}^3/\text{C}$ (solid curves), $F_{12} = 0$ (dotted curves) and $F_{12} = +1 \times 10^{-10} \text{m}^3/\text{C}$ (dashed curves). Other parameters are same as for **Fig. 2**.

The carriers accumulation in the domain wall region is caused by the potential barrier $\varphi(\rho)$ that is in turn caused by the uncompensated bound charge $P_\perp(\rho)$. Corresponding potential barrier is plotted in **Fig. 9a** for positive, zero and negative flexoelectric coupling coefficient F_{12}.
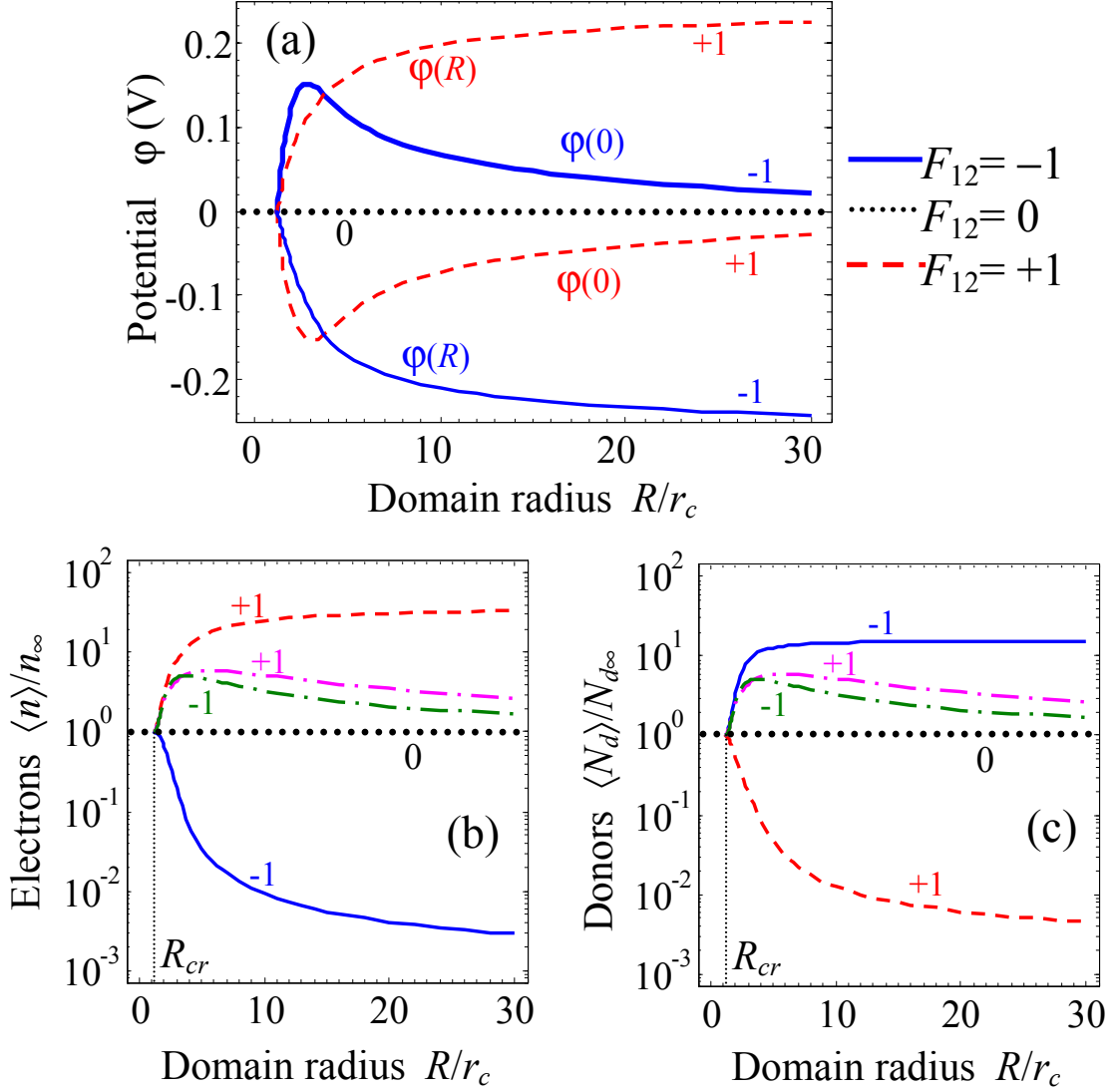

Fig. 9. (Color online) Dependence of the potential φ (a), relative electron density $\langle n(\xi)\rangle/n(\infty)$ (b) and donor concentration $\langle N_d^+(\xi)\rangle/N_d^+(\infty)$ (c) on the radius R of the cylindrical domain calculated for flexoelectric coupling coefficients $F_{12}=-1\times10^{-10}\text{m}^3/\text{C}$, $F_{12}=0$ and $F_{12}=+1\times10^{-10}\text{m}^3/\text{C}$ (numbers "−1", "+1" and "0" near the curves). Potential φ (c) was calculated at the cylindrical domain wall ($\varphi(R)$, solid curves) and in the middle of the domain ($\varphi(0)$, dotted curves). Electron density $n(\rho)$ and donor concentration $N_d^+(\rho)$ were averaged across the domain wall (solid and dashed curves) as well as entire the domain cross-section (dash-dotted curves). Material parameters are the same as in **Figs.2.**

The potential barrier at the curved domain wall monotonically increases with the domain radius R increase and then saturates (see $\varphi(R)$-curves). The potential barrier in the centre of the domain firstly increases with R increase, reaches maximum at $R \sim 3r_c$ and then decreases with further increase of R (see $\varphi(0)$-curves). For sub-micro and microdomains with radius $R \gg 100r_c$ the potential vanishes in the central region of the domain as anticipated.

The size effect of the electron and donor accumulation/depletion by cylindrical domain walls is demonstrated in **Fig. 9b,c** for positive, zero and negative flexoelectric coupling coefficient F_{12}. Similarly to the case of domain stripes, the electronic conductivity of cylindrical domain wall monotonically increases (up to 30 times in comparison with a bulk value) and then saturates with the nanodomain radius increase for positive flexoelectric coupling (see solid curves in **Fig. 9b**). The ionic conductivity of cylindrical domain wall monotonically increases (up to 20 times in comparison with a bulk value) and then saturates with nanodomain radius increase for negative flexoelectric coupling (see dashed curves in **Fig. 9c**).

Similarly to the case of domain stripe, averaging entire the domain cross-section smears the impact of flexoelectric coupling sign (see dash-dotted curves in **Figs.9b,c**). Average densities firstly increase with radius R increase for radii $R_{cr} < R < 5r_c$, then reaches a maximum at $R \sim 5r_c$ and then decreases with further R increase. Electrons and ionized donors accumulation by cylindrical domain is similar to the one discussed in the previous subsection for the case of domain stripes. Average static conductivity of cylindrical nanodomains with radius $r_c \leq R < 10r_c$ appeared essentially higher than the conductivity of the monodomain region due to the flexoelectric coupling.

4. Discussion and summary

Using LGD theory we performed analyses of the carriers' accumulation by 180-degree domain wall in multiaxial ferroelectric-semiconductors with mobile donors. Along with coupled LGD equations for the polarization components, we solved the Poisson equation for the electrostatic potential. Spatial distributions of the ionized shallow donors (e.g. intrinsic oxygen vacancies), free electrons and holes were found self-consistently using the effective mass approximation for their energy density of states. Performed theoretical analyses shows that we meet with several scenarios of the domain wall conduction in stripe and cylindrical domains, depending on the wall geometry (tilt angle, domain shape and size), wall type (head-to-head or tail-to-tail) and the sign and value of the flexoelectric coupling coefficient.

In contrast to uniaxial ferroelectrics, the polarization component perpendicular to the wall plane originates inside the wall region. Similarly to the case of uniaxial ferroelectric-semiconductors [15], the tilted wall is charged in the multi-axial ferroelectric-semiconductors and hence the electric field of

the bound charge attracts free carriers of definite sign and repels the carriers of the opposite sign from the wall region. The carriers' accumulation is highest when the wall plane is perpendicular to the spontaneous polarization direction at the wall (perpendicular domain wall); it decreases with the bound charge decrease and reaches minimum for the parallel domain wall. Carrier accumulation leads to the strong increase of the static conductivity across the charged domain walls in multi-axial ferroelectric-semiconductors, up 3 orders of magnitude for the perpendicular domain walls in $Pb(Zr,Ti)O_3$.

Flexoelectric coupling, which is rather high for ferroelectric perovskites [40-43], leads to the appearance of polarization components perpendicular to the wall plane and its strong gradient across the wall even for nominally uncharged walls. Note, that the perpendicular component appeared in the first principle calculations (see Fig.12 in Ref.[55]). At the same time, the polarization component parallel to the wall plane is indifferent to the presence of the flexoelectric coupling and electrostriction coupling induces the narrowing of the domain wall. The polarization component perpendicular to the wall plane is directly related to the bound charge, in turn leading to a strong electric field at the wall and then to accumulation of free screening carriers across the wall. The carrier accumulation effect by the nominally uncharged domain stripes and cylindrical walls appears to be significant, up to 10-30 times increase for domain stripes and cylindrical nanodomains in $Pb(Zr,Ti)O_3$ for the typical range of flexoelectric coefficients. The charge of accumulated carriers is determined by the sign of the flexoelectric coefficient: positive coefficient leads to the accumulation of negative carriers (electrons or acceptors), negative coefficient leads to the accumulation of positive carriers (holes, donors or vacancies).

The size effect of the electron and donor accumulation by thin stripe domains and cylindrical nanodomains is revealed. In contrast to thick domain stripes and thicker cylindrical domains, in which the carrier accumulation (and so the static conductivity) sharply increases at the domain walls only, nanodomains of radius less then 5-10 correlation length appeared conducting entire their cross-section. Such conductive nanosized channels may be promising for nanoelectronic concepts due to the possibility to control their spatial location by external stimulus (e.g. by nanomanipulation with the charged probe).

Acknowledgements

References

[1] G.I. Guro, I.I. Ivanchik, N.F. Kovtoniuk, Sov. Sol. St. Phys., **11**, 1956-1964 (1969).

[2] J. Seidel, L.W. Martin, Q. He, Q. Zhan, Y.-H. Chu, A. Rother, M. E. Hawkridge, P. Maksymovych, P. Yu, M. Gajek, N. Balke, S. V. Kalinin, S. Gemming, F. Wang, G. Catalan, J. F. Scott, N. A. Spaldin, J. Orenstein and R. Ramesh. Nature Materials 8, 229 – 234 (2009)

[3] J. Seidel, P. Maksymovych, Y. Batra, A. Katan, S.-Y. Yang, Q. He, A. P. Baddorf, S.V. Kalinin, C.-H. Yang, J.-C. Yang, Y.-H. Chu, E. K. H. Salje, H. Wormeester, M. Salmeron, and R. Ramesh, Phys. Rev. Lett. 105, 197603 (2010)

[4] P. Maksymovych et al. (unpublished)

[5] A.A. Grekov, A.A. Adonin, and N.P. Protsenko, Ferroelectrics, 12, 483-485 (1975).

[6] V.Ya. Shur, A.V. Ievlev, E.V. Nikolaeva, E.I. Shishkin, and M.M. Neradovskiy, J. Appl. Phys. 110, 052017 (2011).

[7] A.S. Sidorkin, Domain structure in ferroelectrics and related materials (Cambridge international science publishing, Cambridge, 2006).

[8] A.K. Tagantsev, L.E. Cross, J. Fousek, Domains in Ferroic Crystals and Thin Films. (Dordrecht : Springer, 2010). - 827 p.

[9] V. A. Zhirnov, Zh. Eksp. Teor. Fiz. **35**, 1175 (1958), [Sov. Phys. JETP **35**, 822 (1959)].

[10] W. Cao and L.E. Cross, Phys. Rev. B **44**, 5 (1991).

[11] David A. Scrymgeour and Venkatraman Gopalan, Amit Itagi, Avadh Saxena, and Pieter J. Swart. Phys. Rev. B **71**, 184110 (2005).

[12] Doron Shilo, Guruswami Ravichandran and Kaushik Bhattacharya, Nature Materials 3, 453 - 457 (2004).

[13] V.M. Fridkin, *Ferroelectrics semiconductors*, Consultant Bureau, New-York and London (1980).

[14] M. Y. Gureev, A. K. Tagantsev, and N. Setter Phys. Rev. B 83, 184104 (2011).

[15] E. A. Eliseev, A. N. Morozovska, G. S. Svechnikov, Venkatraman Gopalan, and V. Ya. Shur, Phys. Rev. B **83**, 235313 (2011).

[16] A.K. Tagantsev, E. Courtens and L. Arzel, Phys. Rev. B **64**, 224107 (2001).

[17] B. Houchmandzadeh, J. Lajzerowicz, and E. K. H. Salje, J. Phys. Condens. Matter 4, 9779 (1992).

[18] M.J. Haun, E. Furman, T. R. Halemane and L. E. Cross, Ferroelectrics, 99, 55-62 (1989).

[19] M. Daraktchiev, G. Catalan, J. F. Scott, Ferroelectrics, 375, 122 (2008).

[20] V.G. Bar'yakhtar, V.A. L'vov, D.A. Yablonskii, JETP Lett. 37, 673 (1983).

[21] A.P. Pyatakov and A.K. Zvezdin, Eur. Phys. J. B **71**, 419–427 (2009).

[22] B.M. Darinskii and V.N. Fedosov, *Sov. Phys.- Solid State* **13**, 17 (1971).

[23] J. Hlinka and P. Márton, Phys. Rev. B 74, 104104 (2006).

[24] B. Meyer and D. Vanderbilt, Phys. Rev. B 65, 104111 (2002).

25 Donghwa Lee, Rakesh K. Behera, Pingping Wu, Haixuan Xu, Susan B. Sinnott, Simon R. Phillpot, L. Q. Chen, and Venkatraman Gopalan, Phys. Rev. B **80**, 060102(R) (2009)

26 Liliana Goncalves-Ferreira, Simon A. T. Redfern, Emilio Artacho, and Ekhard K. H. Salje, Phys. Rev. Lett. 101, 097602 (2008).

27. Sh. M. Kogan, Sov. Phys. Solid State 5, 2069 (1964)

28. A.K. Tagantsev, Phys. Rev B, 34, 5883 (1986)

29. A K. Tagantsev, Phase Transitions 35, 119 (1991)

30. V.S. Mashkevich, and K.B. Tolpygo, Zh.Eksp.Teor.Fiz. 31, 520 (1957) [Sov.Phys. JETP, 4, 455 (1957)].

[31]. G. Catalan, L. J Sinnamon, J. M Gregg, J. Phys.: Condens. Matter **16,** 2253 (2004)

[32]. G. Catalan, B. Noheda, J. McAneney, L. J. Sinnamon, and J. M. Gregg, Phys. Rev B **72**, 020102 (2005).

[33] R. Maranganti, N.D. Sharma, and P. Sharma, Phys. Rev. **B 74**, 014110 (2006).

[34] S.V. Kalinin and V. Meunier, Phys. Rev. **B 77**, 033403 (2008).

[35] M.S. Majdoub, P. Sharma, and T. Cagin, Phys. Rev. **B 77**, 125424 (2008).

[36] A.K. Tagantsev, V. Meunier, and P. Sharma, MRS Bull. **34**, 643 (2009).

37. M.S. Majdoub, R. Maranganti, and P. Sharma, Understanding the origins of the intrinsic dead-layer effect in nanocapacitors. Phys. Rev. B **79**, 115412 (2009).

38 E.A. Eliseev, A.N. Morozovska, M.D. Glinchuk, and R. Blinc. Phys. Rev. B. **79**, 165433 (2009).

39 A.N. Morozovska, E.A. Eliseev, G.S. Svechnikov, S.V. Kalinin. Phys. Rev. B **84**, 045402 (2011)

40. W. Ma and L E Cross, Appl. Phys. Lett. 79, 4420 (2001)

41. W. Ma and L E Cross, Appl. Phys. Lett. 81, 3440 (2002)

42. W. Ma and L. E. Cross, Appl. Phys. Lett., 82, 3293 (2003)

43. P. Zubko, G. Catalan, A. Buckley, P. R. L. Welche, and J. F. Scott. Phys. Rev. Lett. 99, 167601 (2007).

44 Sivapalan Baskaran, Xiangtong He, Qin Chen, and John Y. Fu, Appl. Phys. Lett. 98, 242901 (2011).

45 A. N. Morozovska, E. A. Eliseev, M. D. Glinchuk, Long-Qing Chen, Venkatraman Gopalan. Interfacial Polarization in Antidistortive Structures Induced by a Flexoelectric-Rotostriction Product Effect. http://arxiv.org/abs/1108.0019

46 See Supplemental Material at [URL will be inserted by publisher].

47 L.D. Landau and E.M. Lifshitz, Theory of Elasticity. Theoretical Physics, Vol. 7 (Butterworth-Heinemann, Oxford, 1976).

48 V.Y. Shur, Correlated Nucleation and Self-organized Kinetics of Ferroelectric Domains. in "Nucleation Theory and Applications", Ed. by J.W.P. Schmelzer, WILEY-VCH (Weinheim), 2005, Ch.6, pp.178-214.

49 A.N. Morozovska, V. Ya. Shur, et al (unpublished)

50 T.M. J. Haun, Z.Q. Zhuang, E. Furman, S.J. Jang and L.E. Cross. Ferroelectrics, Vol. 99, pp. 45-54 (1989).

51 N.A. Pertsev, V.G. Kukhar, H. Kohlstedt, and R. Waser, Phys. Rev. B **67**, 054107 (2003).

52 W. Ma and L.E. Cross. Appl. Phys. Lett., **88**, 232902 (2006).

53 S.V. Kalinin, B.J. Rodriguez, A.Y. Borisevich, A.P. Baddorf, N. Balke, Hye Jung Chang, Long-Qing Chen, Samrat Choudhury, Stephen Jesse, P. Maksymovych, Maxim P. Nikiforov, and Stephen J. Pennycook Adv. Mater. 22, 314–322 (2010).

54 A.N. Morozovska, E.A. Eliseev, Yulan Li, S.V. Svechnikov, V.Ya. Shur, P. Maksymovych, V. Gopalan, Long-Qing Chen, S.V. Kalinin. *Phys. Rev. B.* 80, P. 214110 (2009).

55 Rakesh K. Behera, Chan-Woo Lee, Donghwa Lee, Anna N. Morozovska, Susan B. Sinnott, Aravind Asthagiri, Venkatraman Gopalan, Simon R. Phillpot. J. Phys.: Condens. Matter **23,** 175902 (2011).